Available online at www.sciencedirect.com
ScienceDirect
Journal of Molecular Catalysis A: Chemical 265 (2007) 133–140
JOURNAL OF MOLECULAR CATALYSIS A: CHEMICAL
www.elsevier.com/locate/molcata

Characterization and photocatalytic activity of K^+-doped TiO_2 photocatalysts

Lung-Chuan Chen [a,*], Chao-Ming Huang [b], Fu-Ren Tsai [a]

[a] *Department of Polymer Materials, Kun-Shan University, Yung Kang City, Tainan 710, Taiwan, ROC*
[b] *Department of Environmental Engineering, Kun-Shan University, Yung Kang City, Tainan 710, Taiwan, ROC*

Received 7 May 2006; received in revised form 3 October 2006; accepted 10 October 2006
Available online 14 October 2006

Abstract

Titanium dioxide doped with K^+ up to 14.3 at.% was prepared by the sol–gel method and thermal treatment. The prepared samples were characterized and subjected to photodegradation of Everdirect Supra Blue BRL dyes (BRL). A mixture of various titanates, $K_{4-4x}Ti_xO_2$, was recognized for the increase in photocatalytic activity. Doping K^+ decreases the crystal size of titanium dioxide, decreases the diminishing rate of surface area with calcination temperature, and increases the calcination temperature required to attain the optimum photocatalytic activity of the sample. TiO_2 doped with 4.6% K^+ and calcined at 973 K shows much higher photoactivity than the other samples when the doping level of K^+ and calcination temperature are 0–14.3% and 673–1273 K, respectively. Photocatalytic degradation of BRL follows the Langmuir–Hinshelwood adsorption model, and the adsorption equilibrium constant and rate constant are 0.0072 min^{-1} and 3.01 ppm/min, respectively. The reaction takes place much effectively at pH 7.2.

Keywords: Titanium dioxide; Potassium ion; Doping; Photocatalytic; Dye

1. Introduction

Semiconductor photocatalysis has been investigated extensively for light-stimulated degradation of pollutants, particularly for complete destruction of toxic and non-biodegradable compounds to carbon dioxide and inorganic constituents [1–4]. Several semiconductors exhibit band-gap energies suitable for photocatalytic degradation of contaminants. Among the photocatalysts applied, titanium dioxide is one of the most widely employed photocatalytic semiconducting materials because of the peculiarities of chemical inertness, non-photocorrosion, low cost and non-toxicity. The photocatalytic process originates from the generation of charge-carriers, electrons (e^-) in the conduction band and holes (h^+) in the valence band, as a result of photoexcitation of semiconductors. The $HO^\bullet$ free radicals, which are recognized as the major oxidant in photocatalytic degradation, are formed by interfacial charge transfer reactions between holes and surface hydroxyl groups or preadsorbed water [5]. On the other hand, the generated holes may recombine with conduction band electrons or get trapped in surface states, lowering significantly quantum efficiency. Therefore, preventing recombination of electrons and holes is crucial to the improvement of the photocatalytic activity of semiconductors. An increase in the charge-carrier lifetime or the interfacial charge transfer rate is expected to raise the quantum efficiency of photocatalysis [6]. Carp et al. [1] cited many references and pointed out that doping semiconductors with various metal ions, composite semiconductors, deposition of noble and group VIII metals, and oxygen reduction catalysts can be employed to enhance photocatalytic efficiency. However, a number of methods, such as impregnation, coprecipitation and sol–gel for preparing photocatalysts and widely varying experimental conditions used for evaluation of photocatalytic activity may lead to controversial influences of modification on photocatalytic systems [7–15]. Iketani et al. [16] cited many reports, and pointed out that some systems demonstrated that metal ion doping could increase photocatalytic activity, whereas others showed detrimental effects. Although a great deal of effort has been devoted to the semiconductor photocatalysis, the detailed mechanism of the modifier reagents affecting photocatalytic

* Corresponding author. Tel.: +886 6 2050137; fax: +886 6 2050540.
E-mail address: lcchen@mail.ksu.edu.tw (L.-C. Chen).

1381-1169/$ – see front matter © 2006 Elsevier B.V. All rights reserved.
doi:10.1016/j.molcata.2006.10.011

activity of semiconductors is still not completely clear. Conclusively, the number of reported photocatalysts that are able to decompose pollutants effectively enough for commercial practice with reasonable activity has been quite limited.

Grzechulska et al. [17] added KOH to a slightly crystallized TiO_2 slurry, followed by thermal treatment, and indicated that KOH/TiO_2 can improve the photocatalytic decomposition of oil. However, little attention has been given to the investigation of the influence of KOH on the characterization and photocatalytic activity of TiO_2.

Textile dyeing and printing industries are the major contributors responsible for the pollution of the aquatic ecosystems since a great quantities of dyes are consumed and the efficiency of dyeing process is low [18]. Accordingly, treatment of residual dyes has been an important issue of research. Although textile dyes can be disposed via some physical and chemical processes, these methods are usually incomplete and ineffective. Additionally, biological processes exhibited limited efficiency due to xenobiotic and non-biodegradable characteristics of textile dyes. Furthermore, some physical and chemical treatments of dyes can generate the second pollution resulting from toxic products [19]. Alternatively, photodegradation of dyes has important practical applications since the complete destruction or mineralization of toxic and non-biodegradable compounds to carbon dioxide and inorganic constituents can be accomplished.

In the present work, BRL is employed as a model compound to examine the photocatalytic activity of K^+-doped TiO_2 prepared via a sol–gel procedure and thermal treatment.

2. Experimental

2.1. Materials

Titanium tetraisopropoxide (TTIP, Acros, 98%), anhydrous ethanol (Scharlace, 99.8%), potassium hydroxide (Shimakyu, EP), hydrochloric acid (Ferak, GR), and Everdirect Supra Blue BRL dyes (BRL, with structure similar to blue 201, a gift from Ever Comp.) were all used as received without purification. Deionized water (18.2 MΩ cm) was obtained from a Millipore Milli Q^+ system.

2.2. Preparation of the K^+-doped TiO_2 photocatalysts

The K^+-doped TiO_2 photocatalysts were prepared in a manner similar to that used for sol–gel. Typically, 20 ml of anhydrous ethanol was added to 9 ml of TTIP, and then the prepared solution was stirred at room temperature on a magnetic stirrer for about 30 min in the dark under nitrogen atmosphere (solution A). At the same time, the desired amount of potassium hydroxide was dissolved into 200 ml of water, and then the solution was stirred for 30 min (solution B). Solution A was added drop by drop to solution B under vigorous stirring. The resulting solution was stirred at 323 K for 24 h, and then the samples were removed from the solution by centrifugation. The obtained samples were dried at 373 K for 24 h and pulverized; subsequently, they were calcined at the desired temperature for 3 h in a programmable furnace (NEY, 3-525). Finally, the calcined samples were ground into fine powder. Samples with 4.6, 6.7, 9.0 and 14.3% mole fractions of K^+ were designated as K1, K2, K3 and K4, respectively. For comparison, pure TiO_2 samples were also prepared with the same procedures as described above, except that solution B contained no potassium hydroxide.

2.3. Characterization of the prepared photocatalysts

The crystalline phases of the prepared samples were identified by X-ray diffraction (XRD) using a Rigaku D/Max III.V X-ray diffractometer with Cu Kα radiation. The crystal size was evaluated from the half-height width of the diffraction peaks at $2\theta = 25.4^\circ$ (1 0 1) and 27.6°(1 1 0) for anatase and rutile phases using the Scherrer equation. Raman spectra of the samples were recorded by a Raman spectrometer (Ventuno, Jasco). Field emission scanning electron microscopy (FESEM) was applied to obtain the microstructure of the prepared sample using a JSM-6700F JEOL microscope. Diffuse reflectance spectroscopy (DRS) was applied to study the threshold wavelengths and absorption intensities of the prepared samples using a UV-Vis spectrophotometer, equipped with an integrated sphere assembly. The specific surface area, *t*-plot micropore surface area, *t*-plot external surface area, pore volume and *t*-plot micropore volume of the prepared samples were measured by the BET and BJH methods according to the nitrogen adsorption–desorption at 77 K on a Micromeritics ASAP 2020 apparatus.

2.4. Photocatalytic activity measurement

Photocatalytic activities of the samples were evaluated in terms of the decolorization of BRL dye under UV irradiation. Photocatalytic testing was conducted in a thermostatic cylindrical Pyrex reactor with a capacity of 500 ml operated at 298 K. A 125 W mercury lamp (HPI 125 W, Philips), with a major emission at 365 nm, was used as the light source. At the beginning of a run, the desired amount of photocatalyst and 250 ml BRL solution were fed into the reactor. Agitation was supplied by a magnetic stirrer rotating rapidly enough to put the reaction into the region of a chemical reaction control. The solution pH was adjusted by dilute HCl and NaOH solutions. The resulting solution was then stirred continuously in the dark for 2 h to achieve the adsorption equilibrium of BRL on the catalyst. Then the photocatalytic run was started by illumination from the light source. Samples were periodically taken from the reactor, centrifuged at 6000 rpm for 10 min, and then filtered through a 0.22 μm membrane filter before being subjected to an UV-Vis spectrophotometer (Hitachi, U-3010).

3. Results and discussion

3.1. Characterization of K^+-doped TiO_2

The specific surface area, *t*-plot micropore surface area, *t*-plot external surface area, pore volume, *t*-plot micropore volume and pore size of K1, K4 and pure TiO_2 samples calcined at 673, 823, 973, and 1123 K are summarized in Table 1. It is obvious that BET surface area, pore volume, external surface

Table 1
Surface areas, pore volumes and pore sizes of the prepared samples with calcination temperature

Samples	Calcination temperature (K)	Surface area (m^2/g)	Micropore surface area[a] (m^2/g)	External surface area[a] (m^2/g)	Pore volume (cm^3/g)	Micropore volume[a] (cm^3/g)	Pore size[b] (Å)
TiO_2-400	673	119.4	1.4	118.0	0.394	–	103.0
TiO_2-550	823	57.7	–	57.7	0.252	–	137.0
TiO_2-700	973	18.8	–	18.8	0.121	–	209.0
TiO_2-850	1123	1.48	1.0	0.5	0.016	–	645.9
K1-400	673	94.2	9.0	85.0	0.300	0.0035	118.1
K1-550	823	60.0	5.9	54.0	0.288	0.0023	177.8
K1-700	973	40.9	5.1	35.8	0.294	0.0021	278.2
K1-850	1123	7.8	1.5	6.3	0.027	0.0006	158.5
K4-400	673	68.3	7.9	60.4	0.249	0.0028	180.3
K4-550	823	25.4	4.3	21.0	0.143	0.0018	242.9
K4-700	973	22.8	2.0	20.8	0.113	0.0007	198.9
K4-850	1123	10.8	2.5	8.3	0.045	0.001	204.2

[a] *t*-Plot method.
[b] BJH adsorption/desorption average pore diameter.

area, micropore surface area and micropore volume decrease with increasing calcination temperature. The surface areas are in the decreasing order of $TiO_2 > K1 > K4$, $K1 > TiO_2 > K4$, $K1 > K4 > TiO_2$, and $K4 > K1 > TiO_2$ when the samples are calcined at 673, 823, 973, and 1123 K, respectively. The dependences of pore volume, micropore volume, external surface area and micropore surface area on the K^+ content and calcination temperature are similar to that of the specific surface area. Dopant K^+ may disperse on or compound with TiO_2, which prevents TiO_2 agglomeration and reduces the diminishing rates of surface area and pore volume with increasing calcination temperature, rendering K^+-doped TiO_2 more porous than plain TiO_2. But this effect may be negligible at 673 K since the agglomeration of TiO_2 arisen from a sintering effect by calcination is insignificant. Consequently, plain TiO_2 exhibits larger surface area than K1 and K4. However, doping K^+ with excess amount may induce the separate particles to coalesce and become a large unit, decreasing surface area and pore volume [10,20]. Hence, surface area and pore volume of K4 are less than those of K1. Further increasing calcination temperature to 1123 K, particle agglomeration caused by a sintering effect exhibits a more significant effect than the K^+ content; therefore, K4 shows larger surface area and pore volume than K1.

Fig. 1 illustrates the XRD patterns of the prepared K1, K4 and pure TiO_2 samples calcined at various temperatures. For pure TiO_2 samples, only the anatase phase is generated after thermal treatment below 823 K as shown in Fig. 1a; further increasing calcination temperature to 973 K leads to formation of 75.8% rutile phase in addition to the anatase phase and furthermore, the anatase phase disappears completely at 1123 K. For K1 samples, on the other hand, the diffraction peaks at corresponding diffraction angles of the anatase phase are much sharpened, and no peak of the rutile phase appears even when calcination temperature increases to 973 K. Roughly 45% of the rutile phase is obtained when the K1 sample is calcined at 1123 K, and the anatase phase disappears completely at 1273 K. These results indicate that doping K^+ would raise the phase transformation temperature of anatase-to-rutile from 973 to 1123 K, which can be ascribed to the interferences of growth of TiO_2 particle by doping K^+. The influence of doping K^+ on XRD patterns is insignificant when calcination temperatures are $\leqq$823 K for the K1 sample, but this influence becomes important with elevating calcination temperature as indicated by new diffraction peaks at $2\theta = 11.58^\circ$, 13.86°, 24.18°, 29.36°, 30.38° and 33.2°, originating from the K_2O/TiO_2 composite, as shown in Fig. 1b. Grzechulska et al. [17] reported that diffraction peaks near $2\theta = 11$–16° and 24–26° were responsible for K_4TiO_4 and $K_2Ti_4O_9$, respectively. Bao et al. [21] indicated that the $K_2O/6TiO_2$ composite exhibited diffraction peaks near $2\theta = 11^\circ$. Furthermore, according to the JCPDS files $K_2Ti_2O_5$ and $K_2Ti_8O_{17}$ show major diffraction peaks at $2\theta = 13.6^\circ, 29.0^\circ$, and 29.2°, and $11.3^\circ, 12.9^\circ, 29.2^\circ$, and 29.7°, respectively. Accordingly, the prepared K^+-doped TiO_2 samples are likely composed of $K_{4-4x}Ti_xO_2$ with x in the range of 0–1. Similar XRD patterns for $K_{4-4x}Ti_xO_2$ complexes were also reported by Liu et al. [22].

Unlike the pure TiO_2 and K1 samples, the diffraction peaks of the anatase and rutile phases of K4 are severely reduced after calcination at 673–1273 K. Although some indistinguishable signals appeared, only a broad and weak band centered at $2\theta = 25.6^\circ$ can be identified, implying the formation of $K_{4-4x}Ti_xO_2$ is insignificant after calcination at 673 K. When calcination temperature increases to 823 K, the anatase bands decrease, and a weak rutile band at $2\theta = 27.6^\circ$ appears, and the bands belonging to $K_{4-4x}Ti_xO_2$ start to grow. Further raising temperature to 973 K, both anatase and rutile bands are reduced and are difficult to differentiate from those for $K_{4-4x}Ti_xO_2$. Then, the XRD bands of $K_{4-4x}Ti_xO_2$ continue to grow with increasing temperature; in contrast, the anatase and rutile phases remain insignificant. These results confirm the existence of $K_{4-4x}Ti_xO_2$ since the anatase and/or rutile phases should be significant if TiO_2 does not compound with K^+. The formation of $K_{4-4x}Ti_xO_2$ complexes in K4 samples is more significant than K1 owing to the high K^+ content, but the formation of anatase and rutile phases in K4 is relatively inhibited. Doping 14.3 at.% K^+ in K4 samples effectively retards growth of TiO_2 crystals by reducing the Ti–O–Ti linkage and developing the Ti–O–K bonding. Consequently, K4 samples mainly consist of $K_{4-4x}Ti_xO_2$ complexes rather than TiO_2 crystals.

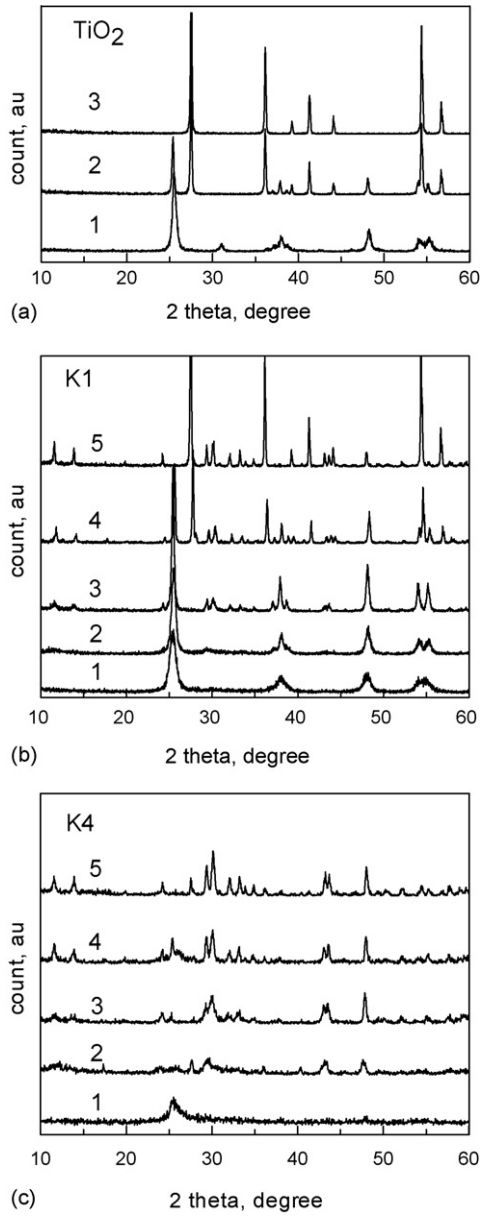

Fig. 1. XRD patterns of the prepared K1, K4 and TiO_2 samples with calcination temperature. (a) TiO_2, line 1: 823 K, line 2: 973 K, line 3: 1123 K. (b) K1, line 1: 673 K, line 2: 823 K, line 3: 973 K, line 4: 1123 K, line 5: 1273 K. (c) K4, line 1: 673 K, line 2: 823 K, line 3: 973 K, line 4: 1123 K, line 5: 1273 K.

The crystal sizes of anatase and rutile phases in the prepared pure TiO_2 and K1 estimated by Scherrer's formula are shown in Fig. 2. The crystal sizes of anatase and rutile phases increase with increasing calcination temperature, and those in K1 are smaller than those of pure TiO_2 since particle agglomeration is retarded by doping K^+.

Fig. 3 demonstrates the Raman spectra of K1, K4 and pure TiO_2 samples. As Alemany et al. [23] and Halary et al. [24] reported, the Raman bands of anatase and rutile phases are located around 150, 200, 395, 515, and 630 cm^{-1}, and 234, 455, and 610 cm^{-1}, respectively. Hence, the bands at 119, 192, 205, 281, 291, 326, 365, 581, 645, and 748 cm^{-1} are attributed to $K_{4-4x}Ti_xO_2$ complexes. Liu et al. [22] studied the solid

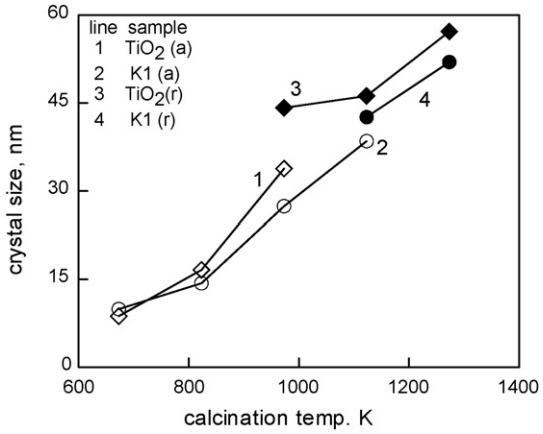

Fig. 2. Crystal sizes of anatase and rutile phases in the prepared pure TiO_2 and K1 samples. Line 1: anatase in pure TiO_2, line 2: anatase in K1, line 3: rutile in pure TiO_2, line 4: rutile in K1.

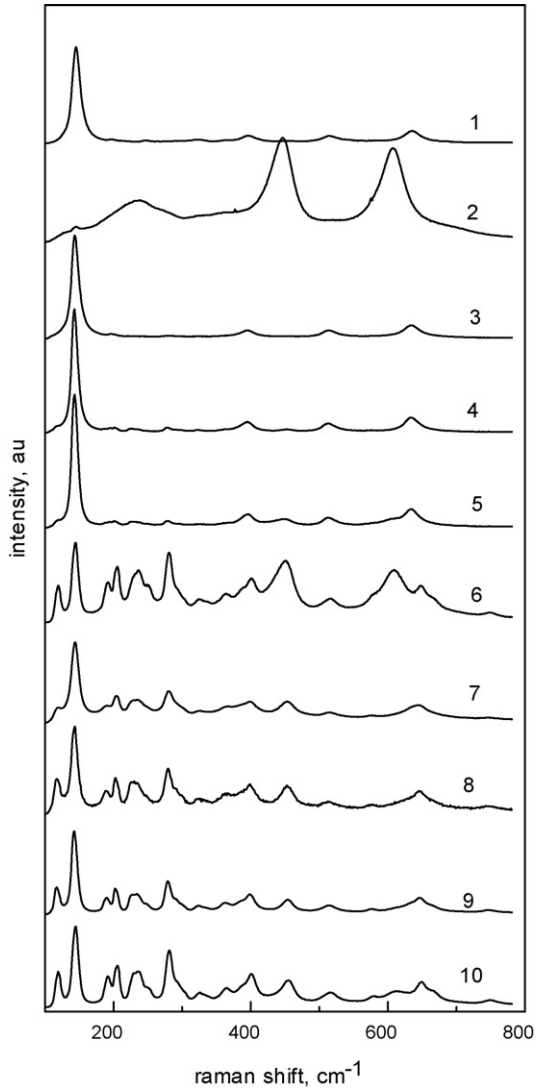

Fig. 3. Raman spectra of the prepared K1, K4 and TiO_2 samples with calcination temperature. Line 1: TiO_2 at 823 K, line 2: TiO_2 at 1273 K, line 3: K1 at 823 K, line 4: K1 at 973 K, line 5: K1 at 1123 K, line 6: K1 at 1273 K, line 7: K4 at 823 K, line 8: K4 at 973 K, line 9: K4 at 1123 K, line 10: K4 at 1273 K.

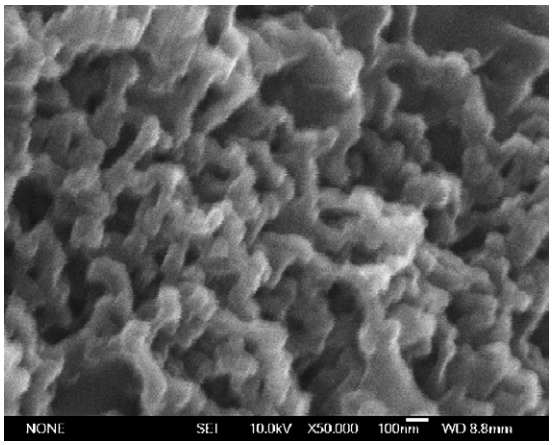

Fig. 4. SEM image of the 973 K-calcined K1 sample.

reaction of TiO_2 and K_2CO_3, and noticed similar Raman spectra for $K_{4-4x}Ti_xO_2$ complexes. It is evident that K4 samples show much more noticeable Raman signals for $K_{4-4x}Ti_xO_2$ than K1, as confirmed by XRD patterns. Although the anatase and rutile phases are insignificant from XRD patterns for K4 samples, Raman spectra show signals close to the anatase and rutile bands as shown in Fig. 3. Moreover, the band near 150 cm^{-1}, representing of the anatase phase, remained after calcination at 1273 K, which is considered high enough to completely transform the anatase phase to the rutile phase. It is suggested that TiO_2 crystalline forms at a lower temperature, followed by a reaction with K^+ to become $K_{4-4x}Ti_xO_2$. However, increasing K^+ decreases and increases the formations of TiO_2 and $K_{4-4x}Ti_xO_2$, respectively. Accordingly, the amount of TiO_2 is maintained at a low level, even below the identifiable limit of XRD. The anatase Raman bands for the 1273 K-calcined samples are suspected to be arisen from the residual anatase remaining after heat treatment since the phase transformation of TiO_2 is retarded by K^+ and/or K_2O.

Fig. 4 shows the SEM images of K1 calcined at 973 K. The observed particle size exceeds the crystal size, indicating that aggregation between particles occurs after calcination at 973 K. The morphology of K1 looks more like a rod than a sphere.

Fig. 5a shows the UV–vis absorption spectra of prepared pure TiO_2 with varying calcination temperature. The threshold wavelength of TiO_2 increases from 388 to 424 nm as calcination temperature increases from 673 to 1273 K. Absorption intensities at 300 and 400 nm, respectively, decrease and increase with increasing calcination temperature. Increasing calcination temperature of TiO_2 increases the rutile phase, which develops a red shift effect and raises absorption intensity at 400 nm. On the other hand, crystal type and surface area are recognized as the important factors affecting absorption intensity at 300 nm. Accordingly, absorption intensity at 300 nm decreases with increasing calcination temperature due to the increase in the rutile phase and decrease in surface area. A shoulder near 385 nm for pure TiO_2 calcined at 973 K is obtained as because both anatase and rutile phases are present in the sample.

The absorption spectra of K1 are similar to those of pure TiO_2, except that the red shift starts to be observable at 1123 K, and the

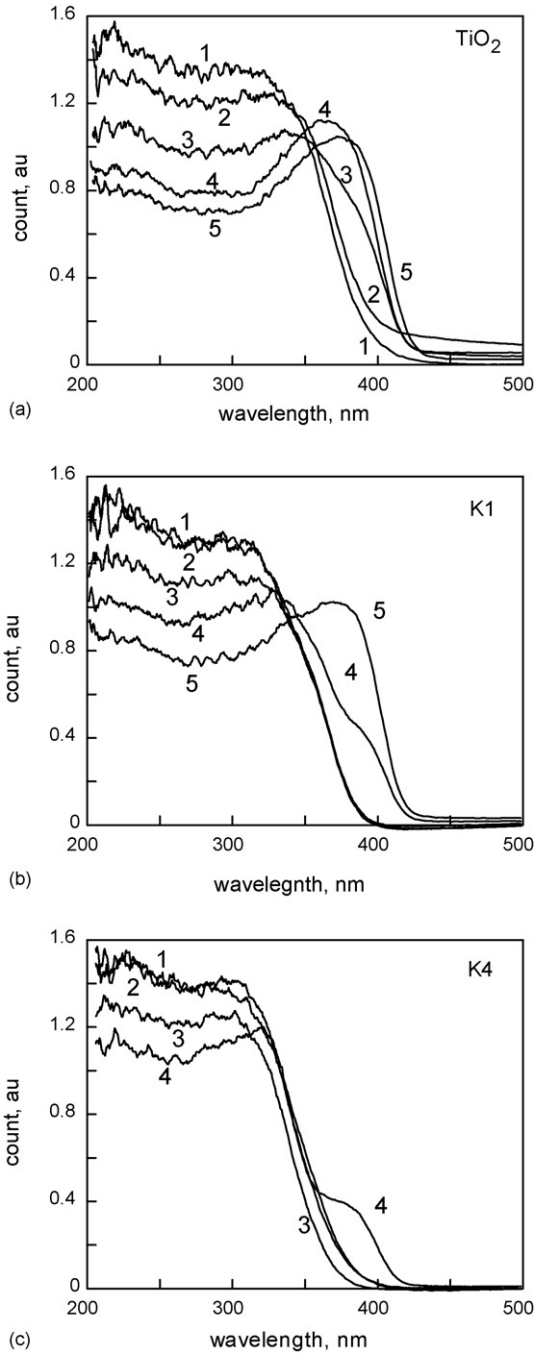

Fig. 5. The UV–vis diffusion reflectance spectra of the prepared TiO_2, K1, K4 samples with calcination temperature. (a) Line 1: 673 K, line 2: 823 K, line 3: 973 K, line 4: 1123 K, line 5: 1273 K. (b) Line 1: 673 K, line 2: 823 K, line 3: 973 K, line 4: 1123 K, line 5: 1273 K. (c) Line 1: 673 K, line 2: 823 K, line 3: 973 K, line 4: 1273 K.

shoulder occurs near 380 nm, as shown in Fig. 5b. An examination of Fig. 5a–c reveals that absorption intensities in the visible and near UV regions and the threshold wavelength decrease in order of $TiO_2 > K1 > K4$. Conversely, the absorption intensity in the far UV region decreases in order of $K4 > K1 > TiO_2$. It seems that $K_{4-4x}Ti_xO_2$ shows insignificant absorption in the visible and near UV regions when compared with TiO_2 crystals; however, $K_{4-4x}Ti_xO_2$ shows enhanced absorption intensity in

the far UV region. The red shift is caused greatly to the rutile phase, and not to the $K_{4-4x}Ti_xO_2$ complex.

3.2. Photocatalytic activity

Effect of pH of BRL solution on UV–vis absorption spectra was examined. The influence of pH on the absorption spectra in the range of 200–800 nm can be negligible when pH increases from 2.8 to 11.6. The maximum absorption wavelength in the visible region is around 576 nm and independent of the pH applied. Hence, 576 nm is taken as the monitoring wavelength to analyze the BRL concentration. Additionally, photolysis of BRL in the absence of photocatalyst was also carried out. The change in absorption intensity of the BRL solution can be neglected during the illuminated period. Hence, the influence of photolysis of BRL can be omitted in the photocatalytic degradation reaction. Adsorption of BRL on the photocatalyst was also studied. After mixing in the dark for 2 h, the adsorption equilibrium of BRL on K1 photocatalyst is established; about 6.0, 13.9, 24.3, 7.2, and 4.1% of the initial BRL are adsorbed on the catalysts calcined at 673, 823, 973, 1123, and 1273 K, respectively. The saturated adsorption amounts of BRL on K1 samples are in the decreasing order of 973 K > 823 K > 1123 K > 673 K > 1273 K. Referring to the surface area of K1 catalyst shown in Table 1 indicates that surface area is not the determining factor affecting the adsorption; furthermore, the crystal phase, type of $K_{4-4x}Ti_xO_2$, pH of point of zero charge (pHpzc), surface morphologies and defective structures of the catalyst are all considered to affect the adsorption performance.

Fig. 6 represents the temporal evolution of the absorption spectra during photocatalytic degradation of the BRL dye in aqueous K1 catalyst suspension. Subsequent illumination causes a continuous decrease in the UV and Vis bands of BRL with increasing irradiation time, which is not accompanied by new absorption bands in the UV–vis region. Moreover, absorption band intensity around 235 nm decreases slowly at 10–30 min

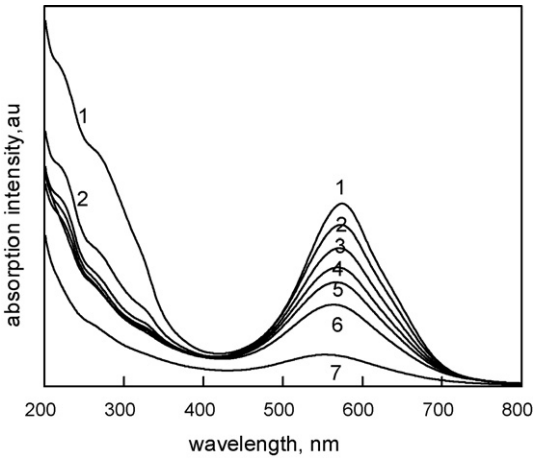

Fig. 6. Evolution of the UV–vis spectra with irradiated time for the photocatalytic degradation of BRL in aqueous solution. Initial pH of the solution: 7.2, initial BRL concentration: 19.5 ± 1.0 ppm, catalyst: K1, catalyst dosage: 1 g/l, volume of solution: 250 ml, line 1: 0 min, line 2: 5 min, line 3: 10 min, line 4: 15 min, line 5: 20 min, line 6: 30 min, line 7: 60 min.

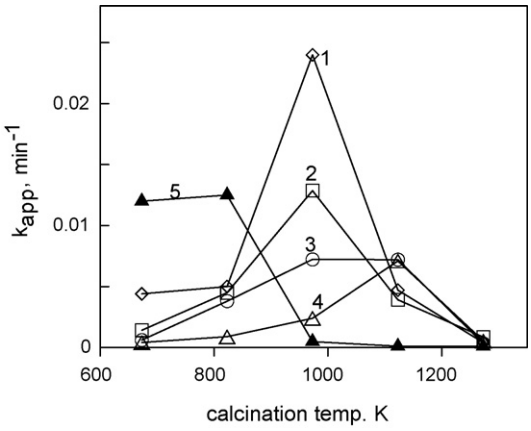

Fig. 7. Plot of k_{app} against calcination temperature for the prepared K1, K2, K3, K4, and pure TiO_2 samples. Catalyst dosage: 1 g/l, initial pH: 7.2, initial BRL concentration: 19.0 ± 1.0 ppm, volume of solution: 250 ml, stir rate: 600 rpm, line 1: K1, line 2: K2, line 3: K3, line 4: K4, line 5: pure TiO_2.

when compared with that at 0–10 min as shown in Fig. 6, implying that the intermediates formed during photodegradation. However, the intermediates can also be degraded by further irradiation.

Usually, photocatalytic degradation of dyes follows the Langmuir–Hinshelwood (L–H) adsorption model for most investigated organic substrates [1]. At a low substrate concentration, the L–H model can be simplified to a pseudo first-order kinetic model, which can be expressed as $\ln(Co/C) = k_{app}t$, where Co is the initial concentration of substrate, C is the concentration of substrate at time t, and k_{app} is the apparent rate constant. The apparent rate constant k_{app} is adopted to describe the photocatalytic activity. Fig. 7 summarizes the effect of the K^+ content and calcination temperature on k_{app}. The optimal calcination temperatures for pure TiO_2, K1, K2, K3 and K4 samples are 823, 973, 973, 1123, and 1123 K, and the corresponding k_{app}s are 0.013, 0.024, 0.013, 0.0072 and 0.0071 min^{-1}, respectively. K1 calcined at 973 K exhibits the highest photocatalytic activity among all samples evaluated. Initially increasing calcination temperature increases k_{app}; however, further increasing temperature decreases k_{app}. Hence, an optimal calcination temperature is accomplished. Furthermore, the optimal temperature increases with increasing doping level of K^+, which is accompanied by a reduction in k_{app}, with the exception of the pure TiO_2 sample. Moreover, k_{app} decreases with increasing K^+ content when calcination temperature is not over the optimal value.

Doping K^+ ions markedly lowers the photocatalytic activity of TiO_2 at 673 and 823 K, which may be ascribed to the development of anatase. This is severely interfered with the dopant and the formation of $K_{4-4x}Ti_xO_2$ is insignificant. Further increasing calcination temperature raises the generation of anatase phase and $K_{4-4x}Ti_xO_2$, thereby increasing the photocatalytic activity of K^+-doped samples up to the optimal temperature, and then k_{app} decreases with increasing temperature since anatase changes into rutile and the surface area of the photocatalyst decreases dramatically.

Increasing the doping level of K^+ decreases the x value of $K_{4-4x}Ti_xO_2$ and increases residual K^+ or K_2O of the samples

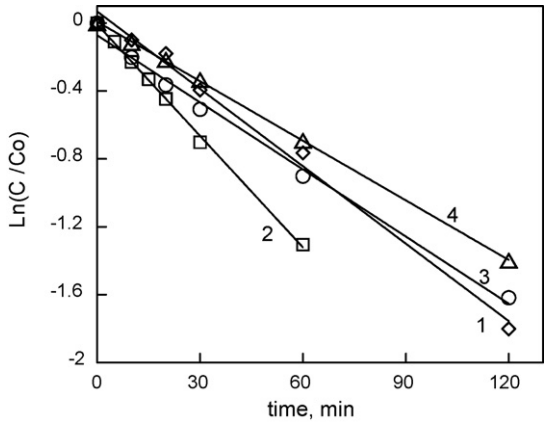

Fig. 8. The logarithmic plot of normalized BRL concentration against photocatalytic time with varying initial pH. Catalyst: K1, catalyst dosage: 1 g/l, initial BRL concentration: 19.0 ± 1.0 ppm, volume of solution: 250 ml, stir rate: 600 rpm, line 1: pH 4.5, line 2: pH 7.2, line 3: pH 9.5, line 4: pH 11.8.

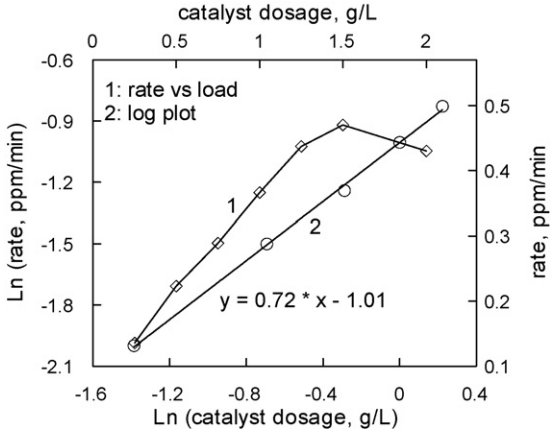

Fig. 9. Effect of catalyst dosage on the photodegradation of BRL. Catalyst: K1, initial pH: 7.2, initial BRL concentration: 19.0 ± 1.0 ppm, volume of solution: 250 ml, stir rate: 600 rpm.

after calcination. Hence a high temperature or a long calcination time is required to develop crystals and to completely transform K^+ and K_2O to $K_{4-4x}Ti_xO_2$. But surface area decreases due to a sintering effect, and the rutile phase develops with elevating temperature. In addition, increasing the doping level also decreases absorption of incident irradiation, and then leads to a detrimental effect on photocatalytic activity. Accordingly, the highly K^+-doped sample shows higher optimal calcination temperature and lower photocatalytic activity than the moderately K^+-doped sample. It is suggested that separate K_2O or K^+ adsorbed on the TiO_2 surface or within the crystal lattice contributes little, or is even harmful, to the photocatalytic activity. Partial substitution of K^+ ions for Ti gives rises to distortion in the lattice structure of TiO_2. Such a distorted TiO_2 surface might have a higher surface energy than pure TiO_2. The promoting effect of proper doping on the photocatalytic activity is considered by reducing the recombination rate between h^+ and e^- pair, enhancing the interfacial charge transfer rate and improving reactants adsorption on the catalyst, and not by increasing absorption of incident irradiation since the absorption intensity decreases with increasing K^+ content. Additionally, alteration of x value in $K_{4-4x}Ti_xO_2$ may also affect photoactivity, but the detailed mechanism is now under investigation.

The role of pH on photocatalytic efficiency was examined in the pH range of 4.5–11.8 using 973 K-calcined K1 as catalyst. The logarithmic plot of normalized BRL concentration against irradiated time is shown in Fig. 8. Subsequently, k_{app} can be obtained from the slope of the straight line on the basis of regression fit. Increasing pH from 4.5 to 7.2 increases k_{app} from 0.015 to 0.023 min^{-1}; however, further increasing pH to 11.8 decreases k_{app} to 0.012 min^{-1}. A maximum photocatalytic activity is attained in the neutral solution. The surface of K1 is strongly affected by pH, and is both positively and negatively charged in the form of protons and hydroxyl ions as pH is below and above the point of zero charge (pHpzc), respectively. Therefore, a low pH is of benefit to adsorption of BRL with a negative charge onto the catalyst; however, it cannot provide enough OH^- ions to react with holes to generate $HO^\bullet$ free radicals, which are regard as the predominant oxidizing species for photocatalytic reactions. On the other hand, increasing pH increases OH^- concentration, thereby enhancing $HO^\bullet$ free radicals; however, the adsorption of BRL onto catalyst is severely reduced. Consequently, an optimal pH is attained to achieve maximum photoactivity [25–31].

Increasing the 973 K-calcined K1 dosage from 0.25 to 1.25 g/l significantly increases the photocatalytic rate from 0.14 to 0.44 ppm/min, and then the reaction rate insignificantly increases to 0.47 ppm/min as the dosage increases to 1.5 g/l; however, the reaction rate decreases to 0.43 ppm/min when the dosage reaches 2 g/l as shown in Fig. 9. The optimal dosage of 1.5 g/l obtained in this work seems reasonable when compared with the dosage in literature [28,31–34]. The optimal catalyst dosage may be affected by several factors, such as volume of the reaction solution, reactor configuration, stir rate, intensity of incident illumination, concentration of reactants, etc. [1,31]. Both adsorption of reactants on the catalyst and absorption of incident photons by the catalyst are enhanced with increasing catalyst dosage initially; hence, the reaction rate increases as the dosage increases. However, a saturated catalyst dosage for maximum absorption of incident photons is achieved at a given intensity of illumination. Thereafter increasing the catalyst dosage cannot further increase the photocatalytic activity, but rather develops a negative influence on the system as a result of a shielding effect and the scattering of incident illumination by the catalyst within the reactor. Accordingly, an optimal photocatalyst dosage is obtained at a specified reaction condition. A straight line with a slope of 0.72 and R^2 of 0.99 is obtained from the logarithmic plot of the photocatalytic rate against catalyst dosage for dosage of 0.25–1.25 g/l, as also shown in Fig. 9. The analytical results indicate that the reaction rate is increased with increasing catalyst dosage to the power of 0.72, which seems reasonable when compared with other systems [26,31,35,36].

Increasing the initial concentration of BRL from 5.7 to 38.4 ppm increases the decolorization rate from 0.12 to 0.66 ppm/min. The reciprocal plot of the rate against the concentration yields a straight line with R^2 of 0.99 as shown in Fig. 10. The slope and intercept are 45.71 and 0.33, respectively. These

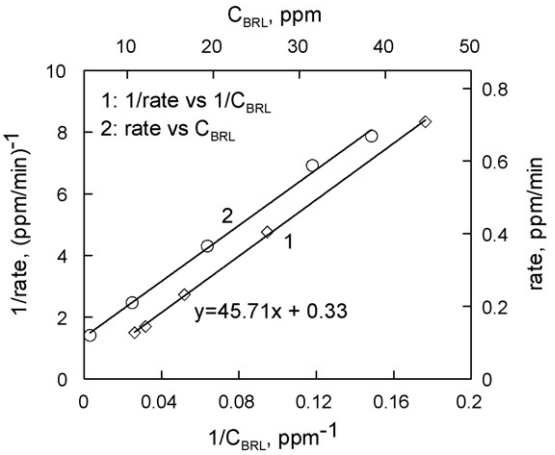

Fig. 10. Effect of initial BRL concentration on the photocatalytic rate. Catalyst: K1, catalyst dosage: 1 g/l, initial pH: 7.2, volume of solution: 250 ml, stir rate: 600 rpm.

results are in good agreement with the Langmuir–Hinshelwood model. The combined expression between the photocatalytic rate, and the catalyst dosage and initial BRL concentration is shown in Eq. (1). The rate constant k is estimated at 3.01 (ppm/min) $(g/l)^{-0.72}$ by the least square technique:

$$R = k\frac{0.0072C}{1 + 0.0072C}(\text{catalyst dosage})^{0.72} \quad (1)$$

4. Conclusion

The K^+-doped TiO_2 synthesized by the sol–gel method from KOH and titanium isopropoxide is more photoactive than plain TiO_2 under some specified conditions. Calcination of K^+-doped TiO_2 leads to the formation of $K_{4-4x}Ti_xO_2$ with multiple x values, which are regarded as promoters of photoactivity. The promotional effect of $K_{4-4x}Ti_xO_2$ is due to reducing recombination of the e^- and h^+ pair, enhancing the interfacial charge transfer and improving reactants adsorption on the catalyst, and not to increasing absorption of incident illumination. Doping TiO_2 with K^+ at appropriate quantities reduces size of TiO_2 crystals, increases surface area and raises the temperature at which anatase changes into the rutile phase. The residual K^+ remaining after calcination shows a detrimental effect on photoactivity. This study reveals that the optimal K^+ amount and calcination temperature for the photoactivity are 4.6% and 973 K, respectively. Photodegradation of BRL follows the Langmuir–Hinshelwood model and is most effective at pH 7.2. The photocatalytic reaction rate is increased with increasing catalyst dosage to the power of 0.72, and the optimal dosage of K1 catalyst is around 1.5 g/l.

Acknowledgement

The authors would like to thank the National Science Council of Taiwan, the Republic of China, for financially supporting this work under Contract No. NSC-93-2745-E-168-005-URD.

References

[1] O. Carp, C.L. Huisman, A. Reller, Prog. Solid State Chem. 32 (2004) 33–177.
[2] M.R. Hoffman, S. Martin, W. Choi, D. Bahnemann, Chem. Rev. 95 (1995) 69–96.
[3] A. Fujishima, T.N. Rao, D.A. Truk, J. Photochem. Photobiol. C: Photochem. Rev. 1 (2000) 1–21.
[4] A. Harastrick, O.M. Kut, E. Heinzle, Environ. Sci. Technol. 30 (1996) 817–824.
[5] J.-M. Herrmann, Catal. Today 53 (1999) 115–129.
[6] Z. Zhang, C.-C. Wang, R. Zakaria, J.Y. Ying, J. Phys. Chem. B 102 (1998) 10871–10878.
[7] W. Choi, A. Termin, M.R. Hoffmann, J. Phys. Chem. 98 (1994) 13669–13679.
[8] A.D. Paola, G. Marci, L. Palmisano, M. Schiavello, K. Uosaki, S. Ikeda, B. Ohtani, J. Phys. Chem. B 106 (2002) 637–645.
[9] M.A. Barakat, H. Schaeffer, G. Hayes, S. Ismat-Shah, Appl. Catal. B: Environ. 57 (2005) 23–30.
[10] J. Zhu, W. Zheng, B. He, J. Zhang, M. Anpo, J. Mol. Catal. A: Chem. 216 (2004) 35–43.
[11] K. Wilke, H.D. Breuer, J. Photochem. Photobiol. A: Chem. 121 (1999) 49–53.
[12] S.T. Martin, C.L. Morison, M.R. Hoffmann, J. Phys. Chem. 98 (1994) 13695–13704.
[13] S. Kiosek, D. Raftery, J. Phys. Chem. 105 (2001) 2815–2819.
[14] D. Dvoranova, V. Brezova, M. Mazur, M.A. Malati, Appl. Catal. B: Environ. 37 (2002) 91–105.
[15] S. Klosek, D. Raftery, J. Phys. Chem. B 105 (2001) 2815–2819.
[16] K. Iketani, R.-D. Sun, M. Toki, K. Hirota, O. Yamaguchi, Mater. Sci. Eng. B 108 (2004) 187–193.
[17] J. Grzechulska, M. Hawerski, W. Morawski, Water Res. 34 (2000) 1638–1644.
[18] P.A. Carneiro, M.E. Osugi, J.J. Sene, M.A. Anderson, M.V.B. Zanoni, Electrochim. Acta 49 (2004) 3807–3820.
[19] H. Lachheb, E. Puzenat, A. Houas, M. Ksibi, E. Elaloui, C. Guillard, J.-M. Herrmann, Appl. Catal. B: Environ. 39 (2002) 75–90.
[20] J.A. Navio, G. Colon, M.I. Bitter, G.N. Bianco, J. Mol. Catal. A: Chem. 106 (1996) 267–276.
[21] N. Bao, X. Lu, X. Ji, X. Feng, J. Xie, Fluid Phase Equilib. 193 (2002) 229–243.
[22] C. Liu, X. Lu, G. Yu, X. Feng, Q. Zhang, Z. Xu, Mater. Chem. Phys. 94 (2005) 401–407.
[23] L.J. Alemany, M.A. Banares, E. Pardo, F. Martin-Jimenez, J.M. Blasco, Mater. Characterization 44 (2000) 271–275.
[24] E. Halary, E. Haro-Poniatowski, G. Benvenuti, P. Hoffmann, Appl. Surf. Sci. 168 (2000) 61–65.
[25] T.C.-K. Yang, S.-F. Wang, S.H.-Y. Tsai, S.-Y. Lin, Appl. Catal. B: Environ. 30 (2001) 293–301.
[26] S. Senthilkumaar, K. Porkodi, J. Colloid Interf. Sci. 288 (2005) 184–189.
[27] N.M. Mahmoodi, M. Arami, N.Y. Limaee, N.S. Tabrizi, Chem. Eng. J. 112 (2005) 191–196.
[28] B. Neppolian, H.C. Choi, S. Sakthivel, B. Arabindoo, V. Murugesan, Chemosphere 46 (2002) 1173–1181.
[29] A. Akyol, H.C. Yatmaz, M. Bayramoglu, Appl. Catal. B: Environ. 54 (2004) 19–24.
[30] C. Lizama, J. Freer, J. Baeza, H.D. Mansilla, Catal. Today 76 (2002) 235–246.
[31] L.-C. Chen, F.-R. Tsai, C.-M. Huang, J. Photochem. Photobiol. A: Chem. 170 (2005) 7–14.
[32] R.P.S. Suri, J. Liu, D.W. Hand, J.C. Crittenden, D.L. Perram, M.E. Mullines, Water Environ. Res. 65 (1993) 665–673.
[33] J.C. Crittenden, J. Liu, D.W. Hand, D.L. Perram, Water Res. 31 (1997) 429–438.
[34] J.M. Herrmann, Catal. Today 24 (1995) 157–164.
[35] K.I. Okamoto, Y. Yamamoto, H. Tanaka, A. Itaya, Bull. Chem. Soc. Jpn. 58 (1985) 2023–2028.
[36] T.-Y. Wei, C.-C. Wan, Ind. Eng. Chem. Res. 30 (1991) 1293–1300.